ARTICLE

# Trop-2, $Na^+/K^+$ ATPase, CD9, PKCα, cofilin assemble a membrane signaling super-complex that drives colorectal cancer growth and invasion

Emanuela Guerra[1,2], Valeria Relli[1], Martina Ceci[1], Romina Tripaldi[1], Pasquale Simeone[1,9,10], Anna Laura Aloisi[1], Ludovica Pantalone[1], Rossana La Sorda[1], Rossano Lattanzio[1,3], Andrea Sacchetti[1,11], Kristina Havas[1,12], Simone Guarnieri[4,5], Daniele Vergara[6], Isabelle Fournier[7], Michel Salzet[7], Nicola Tinari[2], Mauro Piantelli[1,2], Marco Trerotola[1,2,13]✉ and Saverio Alberti[1,8,13]✉



Trop-2 is a transmembrane signal transducer that is overexpressed in most human cancers, and drives malignant progression. To gain knowledge on the higher-order molecular mechanisms that drive Trop-2 signaling, we applied next-generation sequencing, proteomics, and high-resolution microscopy to models and primary cases of human colorectal cancer (CRC). We had previously shown that Trop-2 induces a $Ca^{2+}$ signal. We reveal here that Trop-2 binds the cell membrane $Na^+/K^+$-ATPase, and that clustering of Trop-2 induces an intracellular $Ca^{2+}$ rise followed by membrane translocation of PKCα, which in turn phosphorylates the Trop-2 cytoplasmic tail. This feed-forward signaling is promoted by the binding of Trop-2 to the PKCα membrane-anchor CD9. CRISPR-based inactivation of *CD9* in CRC cells shows that CD9 is required by Trop-2 for recruiting PKCα and cofilin-1 to the cell membrane. This induces malignant progression through proteolytic cleavage of E-cadherin, remodeling of the β-actin cytoskeleton, and activation of Akt and ERK. The interaction between Trop-2 and CD9 was validated in vivo in murine models of CRC growth and invasion. Overexpression of the components of this Trop-2-driven super-complex significantly worsened disease-free and overall survival of CRC patients, supporting a pivotal relevance in CRC malignant progression. Our findings demonstrate a previously unsuspected layer of cancer growth regulation, which is dormant in normal tissues, and is activated by Trop-2 in cancer cells.

*Oncogene*; https://doi.org/10.1038/s41388-022-02220-1

## INTRODUCTION

Trop-2 is a transmembrane glycoprotein that is overexpressed in most human tumors, including colorectal cancer (CRC) [1, 2], and induces growth [2] by triggering converging signaling pathways of Akt [3], Src [4], ERK, NFkB, and cyclin D1 [1, 5].

We recently showed that the wild type (wt) Trop-2 protein acquires oncogenic capabilities upon tumor-specific proteolysis by ADAM10 [6]. However, the molecular determinants that trigger the Trop-2 growth signaling at the plasma membrane of cancer cells remain poorly defined. Here, we investigated the Trop-2 signaling in cancer cells using next-generation sequencing (NGS), proteomics, and high-resolution microscopy. Our findings show that Trop-2 activates a previously unrecognized control layer of cancer cell growth. This occurs by binding of the $Na^+/K^+$-ATPase, which induces the release of intracellular $Ca^{2+}$ through IP3 receptors (IP3Rs) at junctional microdomains. This associates to activation and membrane recruitment of PKCα, which in turn phosphorylates the Trop-2 cytoplasmic tail. This feed-forward signaling is promoted by the physical interaction between Trop-2 and the tetraspanin CD9 at the cell membrane. Trop-2/CD9 binding drives the formation of a protein super-complex, which triggers remodeling of the β-actin/α-actinin/myosin II cytoskeleton through cofilin-1, annexins A1/A6/A11, and gelsolin. We recently reported that Trop-2 induces a PKC-dependent, ADAM10-mediated cleavage of E-cadherin [7, 8], which leads to loss of cell–cell adhesion [9]. We show here that E-cadherin processing is driven by an activated Trop-2 super-complex, and that CD9 is required to carry out this cleavage.

These findings provide a unifying view of Trop-2 in the assembly and activation of a macromolecular membrane super-complex that triggers malignant progression of CRC cells through dynamic interactions of its components at the cell membrane. This signaling module shows clinical relevance in CRC evolution and patient survival, supporting a pivotal impact on CRC malignant progression.

[1]Laboratory of Cancer Pathology, Center for Advanced Studies and Technology (CAST), University "G. D'Annunzio", Chieti, Italy. [2]Department of Medical, Oral and Biotechnological Sciences, University "G. D'Annunzio", Chieti, Italy. [3]Department of Innovative Technologies in Medicine & Dentistry, University "G.D'Annunzio", Chieti, Italy. [4]Laboratory of Cell Physiology, Center for Advanced Studies and Technology (CAST), University "G. D'Annunzio", Chieti, Italy. [5]Department of Neuroscience, Imaging and Clinical Sciences, University "G. D'Annunzio", Chieti, Italy. [6]Department of Biological and Environmental Sciences and Technologies, University of Salento, Lecce, Italy. [7]Inserm U-1192, Laboratoire de Protéomique, Réponse Inflammatoire, Spectrométrie de Masse, Université de Lille 1, Cité Scientifique, Villeneuve D'Ascq Cedex, France. [8]Unit of Medical Genetics, Department of Biomedical Sciences, University of Messina, Messina, Italy. [9]Present address: Department of Medicine and Aging Sciences, University "G. D'Annunzio", Chieti, Italy. [10]Present address: Laboratory of Cytomorphology, Center for Advanced Studies and Technology (CAST), University "G. D'Annunzio", Chieti, Italy. [11]Present address: Josephine Nefkens Institute, Erasmus MC, Rotterdam, The Netherlands. [12]Present address: FIRC Institute of Molecular Oncology (IFOM), Milan, Italy. [13]These authors contributed equally: Marco Trerotola, Saverio Alberti. ✉email: marco.trerotola@unich.it; salberti@unime.it

Received: 1 September 2021 Revised: 10 January 2022 Accepted: 27 January 2022
Published online: 07 February 2022

## RESULTS

### Trop-2 induces intracellular $Ca^{2+}$ rises through binding to $Na^+/K^+$-ATPase

Earlier evidence from our group showed that Trop-2 is a $Ca^{2+}$ signal transducer [10]. However, the related molecular mechanisms remained unknown. Here, time-lapse confocal microscopy imaging of green fluorescent protein (GFP)- or red fluorescent protein (RFP)-engineered $Ca^{2+}$ indicators of human CRC cells (HT-29, KM12SM), showed activation of Trop-2 signaling by cross-linking with the monoclonal antibody (mAb) 162-46.2 [10] (Fig. 1A, B, Supplementary Fig. S1A, B, Supplementary Movie S1). This activatory mAb induced recruitment of Akt—a major Trop-2 effector [3]—to the cell membrane (Supplementary Fig. S1A) and triggered $Ca^{2+}$ signaling. Challenging R-GECO-expressing Trop-2–positive cells with RS-7—an anti-Trop-2 mAb developed into the antibody-SN-38 drug conjugate Sacituzumab govitecan-hziy (Trodelvy) [11, 12]—did not induce any increase of $Ca^{2+}$ levels (Supplementary Fig. S1C). Adding 162-46.2 to cells after the failed stimulation with RS-7 led to full-blown intracellular $Ca^{2+}$ signaling (Supplementary Fig. S1C), supporting stereochemical specificity of Trop-2 signaling triggers [10].

To explore how Trop-2 induced intracellular $Ca^{2+}$ waves, we assessed the impact of removing $Ca^{2+}$ ions from the culture medium, and of inhibiting the IP3Rs with the antagonist 2-aminoethyl diphenylborinate (2-APB), before administration of 162-46.2 mAb. Extracellular $Ca^{2+}$ removal (Fig. 1C, blue curve) or chelation (Supplementary Fig. S1D) led to a delayed and smaller increase of intracellular $Ca^{2+}$ upon antibody cross-linking, while pre-incubation with 2-APB completely abolished the intracellular $Ca^{2+}$ wave (Fig. 1C, red curve). Hence, Trop-2-driven $Ca^{2+}$ signal transduction is predominantly based on the release of $Ca^{2+}$ from intracellular stores.

Trop-2 is not a $Ca^{2+}$ channel [10, 13–15]. We thus hypothesized that Trop-2 acted as a regulator of a $Ca^{2+}$ channel. Trop-2-binding molecules were sought by nanoscale liquid chromatography/mass spectrometry (NanoLC/MS) analysis of Trop-2 immunoprecipitates from CRC cells. This led to identify the α1 subunit of the $Na^+/K^+$-ATPase as a Trop-2 interactor (Supplementary Table S1A, B), as confirmed by Western blotting analysis of cell membrane co-immunoprecipitated material (Fig. 1D). The $Na^+/K^+$-ATPase regulates $Ca^{2+}$ influx through the $Na^+/Ca^{2+}$ exchanger (NCX) [16]. However, the $Na^+/K^+$-ATPase also has non-pumping functions [17], as mediated by the tethering of Src, phospholipase C (PLC) and IP3Rs into junctional calcium signaling microdomains, that induce $Ca^{2+}$ release from internal stores [18, 19]. Cardiotonic steroids, such as ouabain, bind the $Na^+/K^+$-ATPase and inhibit its ion-pumping function, while modulating downstream signaling cascades, including a bi-modal activation/inhibition of Src [20–26]. Consistent with a role of Trop-2 as stimulator of Src activity [4], treatment of KM12SM [27] and HT-29 CRC cells with ouabain inhibited the growth of HT-29/Trop-$2^{low}$ [9] and of KM12SM/vector cells, but did not suffice to inhibit the growth of HT-29/Trop-$2^{high}$ [9] and of KM12SM/Trop-2 cells (Fig. 1E and Supplementary Fig. S1E).

### The Trop-2 $Ca^{2+}$ rise stimulates a Trop-2/PKCα feed-forward activatory signaling

$Ca^{2+}$-activated Trop-2 effectors were searched through global proteomic and phosphoproteomic analysis (Supplementary Fig. S2A, Supplementary Table S1C). Among top-scoring kinases we revealed the protein kinase C (PKC) family (Supplementary Table S1C, D), which was formerly reported to activate Trop-2 signaling [28–30]. $Ca^{2+}$-dependent PKCα [31] quantitatively stood out among the Trop-2–modulated PKCs (Supplementary Table S1C, D). Consistently, stimulation of Trop-2 with 162-46.2 was found to induce translocation of PKCα-GFP toward Trop-2 sites at cell–cell junctions and at free membrane rims (Fig. 2A, Supplementary Fig. S2B, Supplementary Movie S2). $Ca^{2+}$-independent PKCδ and PKCε [31] remained diffusely cytoplasmic upon Trop-2 cross-linking, whereas both of these PKC isoforms were efficiently recruited to the plasma membrane upon treatment with ATP (Supplementary Fig. S2C). As predicted, the membrane recruitment induction ($5.0 \pm 0.5$ s) and recovery ($55.2 \pm 10.6$ s) dynamics of PKCα-GFP closely followed those of $Ca^{2+}$ signals. Notably, Trop-2–induced membrane recruitment of PKCα-GFP was abolished by inhibiting the increase of the intracellular $Ca^{2+}$ levels through pre-incubation with 2-APB (Fig. 2B, top), or with U73122, which blocks PLC-dependent conversion of phosphatidylinositol bisphosphate ($PIP_2$) to inositol trisphosphate ($IP_3$) (Fig. 2B, bottom). $Ca^{2+}$-dependent translocation of PKCα to the cell membrane leads to PKCα activation via phosphorylation at Ser657 (P-PKCα). Consistently, Trop-2 expression induced increase of P-PKCα (Fig. 2C) and accumulation of activated PKCα at the plasma membrane, where it tightly colocalized with Trop-2 (Fig. 2D).

The cytoplasmic tail of Trop-2 contains a PKC phosphorylation site at Ser303 [28] within the HIKE region, a consensus motif for regulatory protein-protein and protein-phospholipid interactions [32, 33]. Deletion of the HIKE region (Trop-2_ΔHIKE) prevented Trop-2 from recruiting PKCα to the cell membrane (Fig. 2E), despite preservation of the Trop-2-induced intracellular $Ca^{2+}$ rise (Fig. 2F), suggesting that the Trop-2 HIKE region is a key docking site of PKCα at the cell membrane.

Stimulation of HT-29 cells with the PKC activator phorbol 12-myristate 13-acetate (PMA) prompted PKCα-EGFP translocation to Trop-2-mCherry sites at cell–cell contacts (Supplementary Fig. S2D), suggesting a feed-forward, pro-growth signaling between Trop-2–driven activation of PKCα and PKCα-mediated phosphorylation of the Trop-2 cytoplasmic tail. Trop-2 phosphorylation was induced by PMA (3.9 [±1.5]-fold vs. basal), and PMA-driven phosphorylation was effectively inhibited by overexpression of a dominant-negative (DN) PKCα mutant, PKCα_K368R (Fig. 3A). Trop-2_ΔHIKE did not stimulate growth, nor did the Ser303 to Ala (S303A) mutant (Fig. 3B), indicating that Trop-2 phosphorylation at S303 by PKCα is an obligate step for growth induction. siRNA-mediated down-regulation of PKCα or overexpression of DN-PKCα correspondingly abolished growth stimulation by Trop-2, with no effect observed in Trop-2–null control cells (Fig. 3C and Supplementary Fig. S3A). Overexpression of wtPKCα did not suffice to stimulate growth of Trop-2–null cells (Supplementary Fig. S3A). On the other hand, overexpression of a constitutively active PKCα variant devoid of the regulatory domain (CAT-PKCα) induced a stimulation of Trop-2–null cell growth that was comparable to that of Trop-2, whereas CAT-PKCδ had no effect (Supplementary Fig. S3A). This indicated that a functional Trop-2/PKCα feed-forward activatory phosphorylation is required to stimulate cell growth.

Recent findings have shown that Trop-2 can be phosphorylated at the Ser322 residue [30]. Our data confirmed Trop-2 phosphorylation at S322 (Fig. 3). Besides S303 and S322, no other phosphorylation sites appeared viable, as the double mutation S303A–S322A entirely abolished phosphorylation on the Trop-2 tail (Fig. 3D). S303A or S322A single mutations prevented cell growth stimulation by Trop-2, indicating that a two-pronged phosphorylation of both S303 and S322 is required for growth induction (Fig. 3B). However, the double mutant S303A–S322A (Supplementary Fig. S3B) was as efficient as wtTrop-2 at inducing an intracellular $Ca^{2+}$ rise (Fig. 3E), indicating that $Ca^{2+}$ signaling is not sufficient for growth induction. Our previous findings showed that Trop-2 stimulates the activity of Akt and ERK, and that this was required for inducing cell growth [1–3]. Consistent, the double mutant S303A–S322A abolished the Trop-2-induced activatory phosphorylations of ERK1/2 and Akt, confirming that phosphorylation of the Trop-2 cytoplasmic tail at S303 and S322 is an obligate step in cell growth induction (Fig. 3F).

### The Trop-2/PKCα feed-forward signaling is activated by mTOR

The mammalian target of rapamycin complex 2 (mTORC2) phosphorylates Akt at Ser473 [34] and PKCα at the turn and

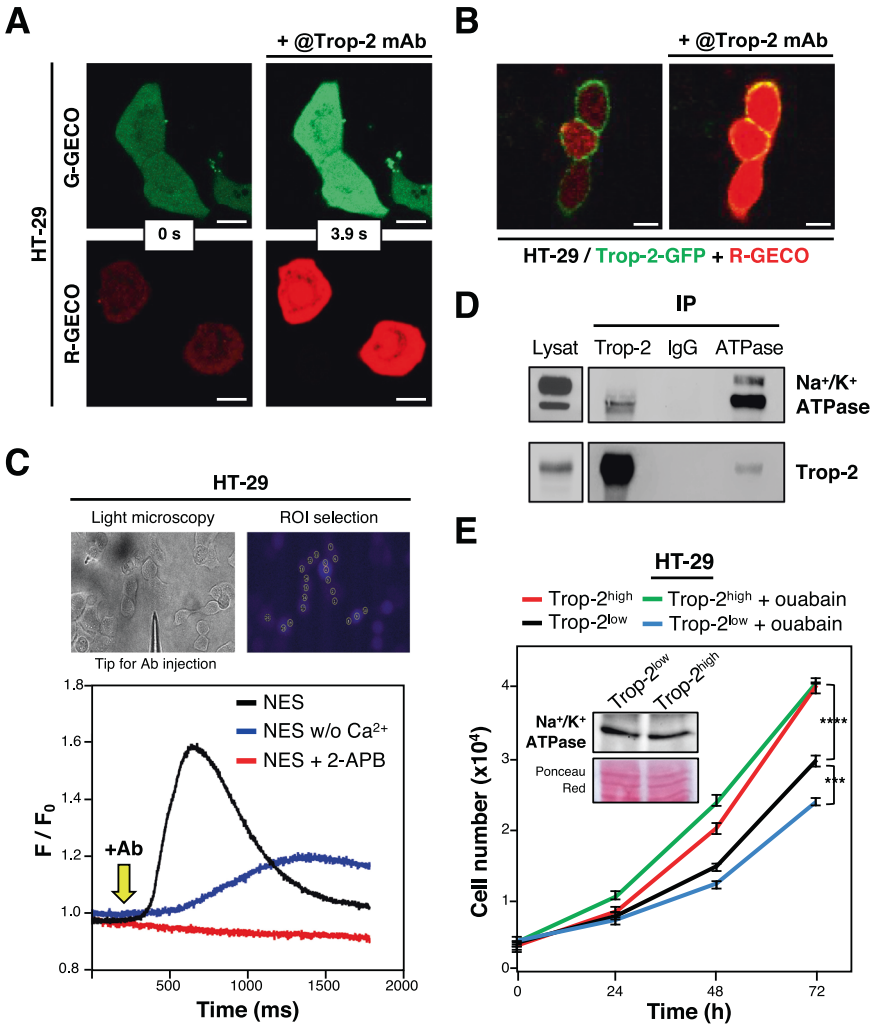


**Fig. 1 Trop-2 induces intracellular $Ca^{2+}$ rise through $Na^+/K^+$-ATPase. A** Confocal time-lapse microscopy of HT-29 CRC cells transfected with CMV-G-GECO1.2 (top) and CMV-R-GECO1.2 (bottom), upon cross-linking of Trop-2 with the 162-46.2 mAb. Scale bars, 10 μm. **B** Confocal time-lapse microscopy of HT-29 cells co-transfected with Trop-2-GFP and CMV-R-GECO1.2, upon cross-linking of Trop-2 with the 162-46.2 mAb. Scale bars, 10 μm. **C** Intracellular $Ca^{2+}$ variations of HT-29 cells in response to stimulation with the 162-46.2 anti Trop-2 mAb. The anti Trop-2 mAb was microinjected in the area surrounding the tip (top panel, left), and quantification of the fluorescence was performed in multiple regions-of-interest (ROI) per assay (top panel, right) as described in "Material and methods". Fluorescence values during time were plotted to compare the various conditions (bottom panel). **D** Immunoprecipitation on HT-29 cells using IgG of irrelevant specificity (IgG) or mAb targeting Trop-2 (Trop-2) or $Na^+/K^+$ ATPase α1. The presence of the $Na^+/K^+$ ATPase (top) and of Trop-2 (bottom) in the HT-29 protein lysate and in the co-immunoprecipitates was revealed by Western blotting. **E** HT-29/Trop-$2^{low}$ and HT-29/Trop-$2^{high}$ cells were subjected to treatment with 10 nM ouabain every 24 h, and monitored for their growth in vitro for up to 72 h. Bars, SEM. ****$P < 0.0001$; ***$P < 0.001$. *Inset*, Western blotting analysis of $Na^+/K^+$ ATPase expression levels in HT-29/Trop-$2^{low}$ and HT-29/Trop-$2^{high}$ cells. Ponceau Red, control of protein loading.

hydrophobic motifs [35], with downstream up-regulation of the Trop-2 effector NFkB [1, 36]. Treatment of HT-29/PKCα-GFP cells with the mTORC2 inhibitor PP242 prevented Trop-2–induced translocation of PKCα to the cell membrane, in a dose-related manner (Supplementary Fig. S3C and Supplementary Movie S3). Consistently, inhibition of the mTORC2 complex through shRNA-mediated downregulation of Sin1 expression (Supplementary Fig. S3D) or treatment with PP242 resulted in abrogation of the Trop-2 contribution to the growth of KM12SM cells (Supplementary Fig. S3E). Collectively, these data demonstrate that mTORC2 is the upstream mediator of the Trop-2/PKCα feed-forward activatory signaling, and is required for driving PKCα-mediated phosphorylation of the Trop-2 tail for the activation of Akt and ERK.

### Cytoskeleton organizers orchestrate Trop-2 signaling

mTORC2 regulates the organization of the actin cytoskeleton through PKCα [37]. We recently demonstrated that Trop-2 induces ADAM10-mediated cleavage of the E-cadherin intracellular domain [9], which leads to detachment of E-cadherin from the β-actin cytoskeleton, to destabilization of cell–cell adhesions and to enhanced CRC invasion [9] and cell migratory phenotypes [4, 38, 39].

Here, we carried-out 2D-PAGE, tandem mass spectrometry (MS/MS) and Western blotting analysis of Trop-2 immunoprecipitates in order to define the Trop-2 cytoskeletal interactome. These assays revealed gelsolin, cofilin-1, myosin isoforms, myosin regulatory light chain (MRLC) (Fig. 4A and Supplementary Table S1A, B) and annexins A1/A11 (Fig. 4B and Supplementary Fig. S4A) as major cytoskeletal components of this Trop-2 assembly. The expression levels of distinct cytoskeleton components, such as annexin A6, gelsolin-like capping protein and Cdc42 were found modulated by Trop-2 (Supplementary Fig. S2A, and Supplementary Table S1C).

Trop-2 overexpression induced phosphorylation of cofilin-1 at Ser-3 (Fig. 4C). Dephosphorylated/active cofilin-1 binds $PIP_2$ at the

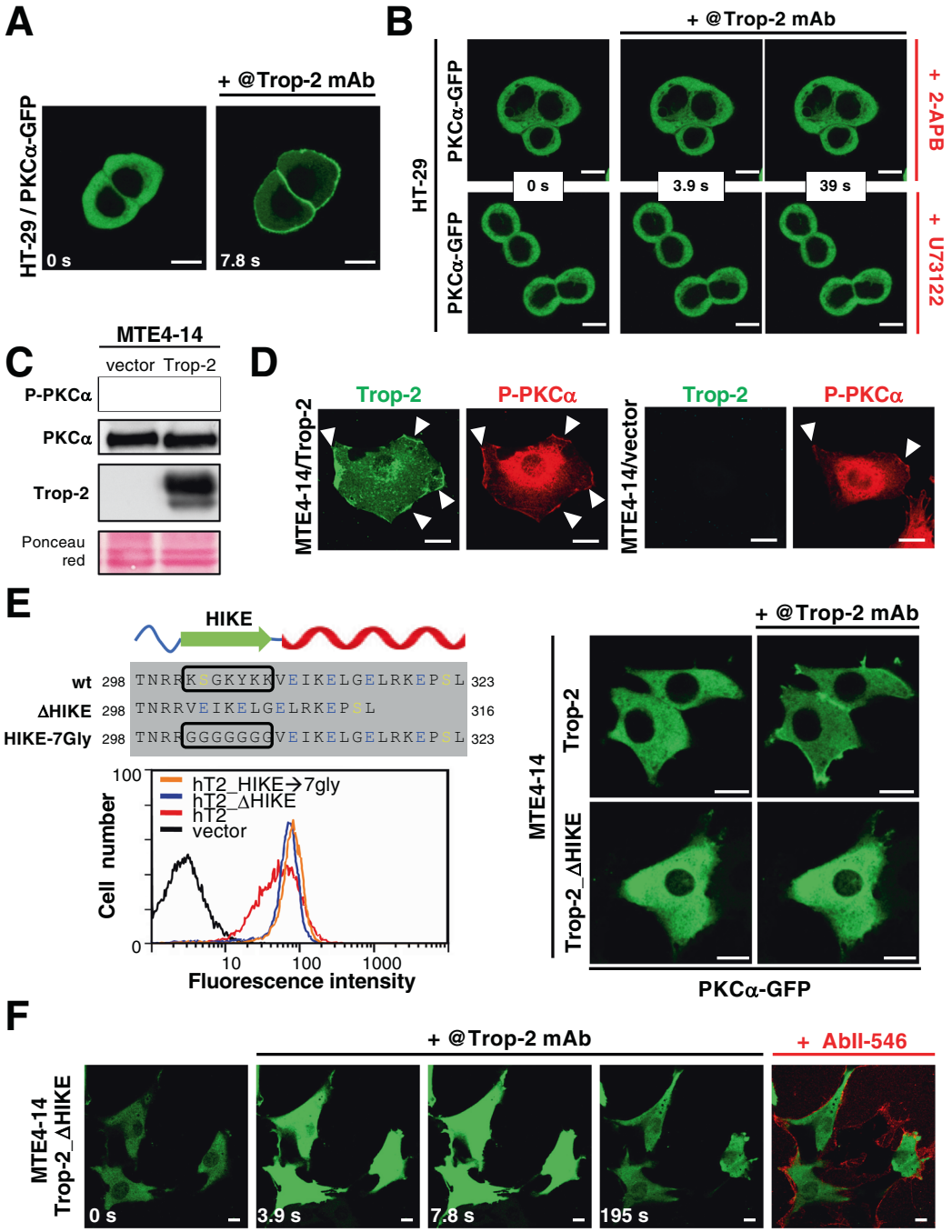


**Fig. 2 The Trop-2 cytoplasmic tail is required for PKCα recruitment to the cell membrane but not for intracellular $Ca^{2+}$ rise. A** Confocal time-lapse microscopy of HT-29 cells transiently transfected with PKCα-GFP, before (left) and after (right) cross-linking of Trop-2 with the 162-46.2 mAb. Scale bars, 10 μm. **B** Confocal time-lapse microscopy of HT-29/PKCα-GFP transfectants. Cells were preincubated with 2-APB (top panel) and U73122 (bottom panel) before Trop-2 cross-linking with the 162-46.2 mAb. Scale bars, 10 μm. **C** Western blotting analysis showing the expression levels of P-PKCα (S657), total PKCα, and Trop-2 in MTE4-14/vector and MTE4-14/Trop-2 transfectants. Total PKCα and Ponceau Red staining were used as controls of protein loading. **D** (*arrowheads*) Confocal microscopy analysis of membrane localization of Trop-2 (green) and P-PKCα (red) in MTE4-14/Trop-2 and MTE4-14/vector. Scale bars, 10 μm. **E** *Left* Cytoplasmic tail sequences of wtTrop-2 and HIKE mutants (top panel). Black box: HIKE sequence; yellow: serines; blue: glutamic acids. Flow cytometry analysis of KM12SM cells transfected with the empty vector, wtTrop-2, Trop-2_ΔHIKE, and Trop-2_HIKE-7Gly (bottom panel). The T16 anti Trop-2 mAb was used for live-cell staining. **E** *Right* Confocal time-lapse microscopy of MTE4-14/Trop-2 (top panels) and MTE4-14/Trop-2_ΔHIKE (bottom panels) transfected with PKCα-GFP, upon cross-linking of Trop-2 with the 162-46.2 anti-Trop-2 mAb, as indicated. Frame at 15.6 s after mAb administration is shown. No PKCα-GFP membrane recruitment in MTE4-14/Trop-2_ΔHIKE was observed along the entire time-lapse. Scale bars, 10 μm. **F** Confocal time-lapse microscopy of MTE4-14/Trop-2_ΔHIKE cells transfected with CMV-G-GECO1.2, upon cross-linking of Trop-2 with the 162-46.2 anti-Trop-2 mAb. Time frames at 3.9, 7.8, and 195 s after mAb administration is shown. At the end of the assay, a secondary anti-mouse Ab conjugated to AlexaFluor 546 was added to the cells to reveal the 162-46.2 primary mAb/localization of Trop-2_ΔHIKE (red). Scale bars, 10 μm.

plasma membrane [40]. Hydrolysis of $PIP_2$ into $IP_3$ and diacylglycerol by PLC is followed by translocation of active cofilin-1 to F-actin, for severing of the actin polymers. Actin filaments with free barbed ends and cofilin–G-actin complexes then diffuse in the cytoplasm, where cofilin-1 is phosphorylated (and inactivated) by the LIM kinase (LIMK) [41], which is modulated by Trop-2 through PAK4 [39]. Cofilin-1 phosphorylation/dephosphorylation are critical for ensuring a regulated turnover of the actin filaments. We showed that Trop-2 regulates actin microfilament rearrangement, as stimulation with 162-46.2 leads to rapid disappearance of the cortical actin signal, followed by recovery of F-actin localization at the plasma membrane (Fig. 4D and Supplementary Fig. S4B). PKCα can contribute to cofilin-1 inactivation by phosphorylation at its Ser23-Ser24 residues [42]. Hence, membrane recruitment of PKCα upon Trop-2 cross-linking was predicted to promote equilibrium recovery and restoration of cortical F-actin. Consistently, immunofluorescence analysis of P-PKCα and β-actin revealed co-localization with Trop-2 at the cell membrane (Supplementary Fig. S4C). Furthermore, simultaneous acquisition of PKCα-GFP and Lifeact-mRFP1 upon cell treatment with the 162-46.2 mAb revealed a rapid recruitment of PKCα to the cell membrane, followed by β-actin repolymerization (14.4 ± 4.5 s) (Supplementary Movie S4). Polymerization of cortical actin fully recovered after induction of Trop-2 signaling (at 54.4 ± 11.2 s). This process was strongly reduced in cells that expressed the Trop-2_ΔHIKE mutant (Supplementary Fig. S4D), supporting our model of a

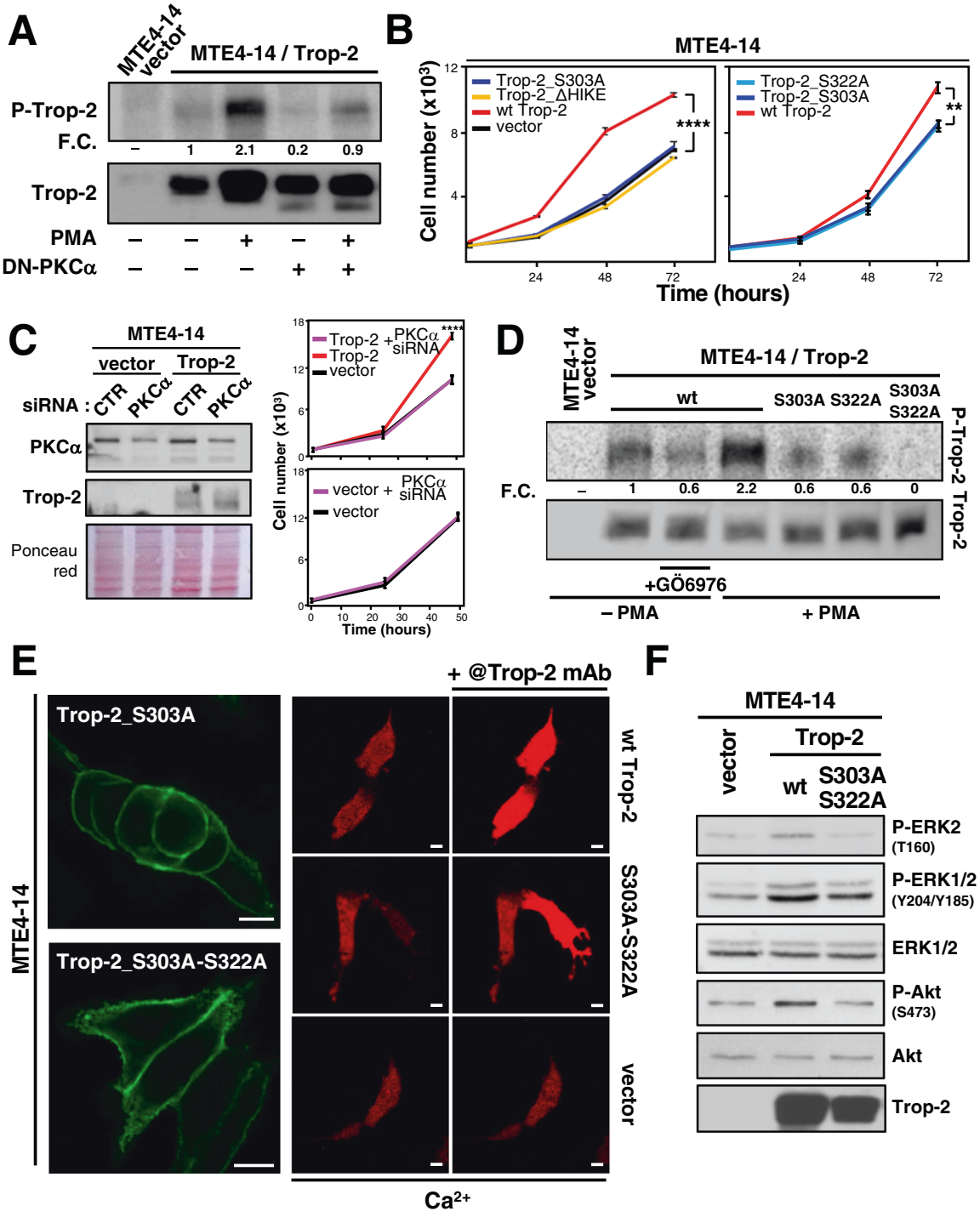

**Fig. 3 The Trop-2/PKCα feed-forward signaling. A** Phosphoimaging of phosphorylated Trop-2 (P-Trop-2; top) immunoprecipitated from MTE4-14/Trop-2 transfectants previously labeled with [$^{32}$P]-orthophosphate in basal conditions or in the presence of the PKCα activator PMA, alone or combined with overexpression of the inactive DN-PKCα. Absolute Trop-2 levels (bottom) in the immunoprecipitated material for each condition were quantified by Western blotting and were used to normalize phosphorylation fold changes (F.C.) **B** In vitro cell growth of MTE4-14 transfectants. S303A (dark blue), S322A (light blue), and ΔHIKE (yellow) Trop-2 mutants, wtTrop-2 (red) and vector-only (black) transfectants are shown. Bars, SEM. $^{**}P < 0.01$ and $^{****}P < 0.0001$ (MTE4-14/Trop-2 vs. other groups). **C** *Left* Western blotting analysis of PKCα and Trop-2 in MTE4-14/vector and MTE4-14/Trop-2 cells upon transfection with specific (siPKCα) or control (siCTR) siRNA vectors. Ponceau Red staining is shown as control of protein loading. **C** *Right* Growth curves of MTE4-14/Trop-2 and MTE4-14/vector cells transfected with siPKCα and siCTR vectors. Bars, SEM. $^{****}P \leq 0.0001$ (MTE4-14/Trop-2 vs. other groups). **D** Phosphoimaging of phosphorylated wt or mutagenized Trop-2 (P-Trop-2, top) immunoprecipitated from MTE4-14 transfectants previously labeled with[$^{32}$P]-orthophosphate in basal conditions or in the presence of PMA and/or with the PKCα inhibitor GÖ6976. Absolute Trop-2 levels (bottom) in the immunoprecipitated material for each condition were quantified by western blotting and used to normalize the phosphorylation fold changes. **E** *Left* Fluorescence confocal microscopy of MTE4-14/Trop-2_S303A (top) and MTE4-14/Trop-2_S303A-S322A (bottom) transfectants. Scale bars, 10 μm. **E** *Right* Confocal time-lapse microscopy of MTE4-14/Trop-2 (top), MTE4-14/Trop-2_S303A-S322A (mid), and MTE4-14/vector (bottom) transfected with CMV-R-GECO1.2, before (left) and after (right) cross-linking of Trop-2 with the 162-46.2 mAb. Time frames at 3.93 s are shown. Scale bars, 10 μm. **F** Western blotting analysis showing the expression levels of P-ERK1/2, total ERK1/2, P-Akt, total Akt and Trop-2 in MTE4-14 cells transfected with empty vector, wt Trop-2 and Trop-2_S303A-S322A. Total Akt and Erk1/2 are also used as controls of protein loading.

cofilin-dependent depolymerization of cortical actin through the $Na^+/K^+$ ATPase/Src/PLC/IP3R axis, followed by actin repolymerization through PKCα-mediated inactivation of cofilin-1.

Formation and turnover of nascent adhesions at the leading edge of migrating cells are finely tuned by the coordinated action of two actin cross-linking proteins, α-actinin and myosin II [43, 44]. Our findings showed that Trop-2 binds MRLC and induces MRLC activatory phosphorylation at Ser19 [3], which is known to stimulate myosin II filament assembly and motor activity [45]. Cross-linking of Trop-2 induced recruitment of myosin IIa-mTFP1 (39.9 ± 11.2 s) at the plasma membrane, with overlapping kinetics vs. β-actin repolymerization (Supplementary Fig. S4F). Our previous studies revealed a binding site for α-actinin in the C-terminus of Trop-1/EpCAM, a paralogous molecule of Trop-2 [14, 46]. Proteomic analysis of Trop-2 immunoprecipitates revealed that α-actinin binds Trop-2 (Supplementary Table S1A, B), and fluorescence confocal time-lapse microscopy showed that α-actinin-GFP is recruited to the cell membrane upon cross-linking of Trop-2 (Supplementary Fig. S4E). Consistently, cytochalasin D (an inhibitor of β-actin polymerization) induced release of Trop-2–activated/membrane-recruited downstream effectors, such as P-PKCα and P-ERK (Supplementary Fig. S4G).

## Trop-2 associates with CD9 and recruits PKCα at the cell membrane

At the plasma membrane, the association of PKCs to tetraspanins —such as CD9—allows these kinases to be recruited into proximity of various transmembrane receptors for regulating their activity [47, 48]. CD9 mediates $Ca^{2+}$—induced keratinocyte differentiation and motility through interaction with E-cadherin and activation of PI3K/Akt [49]. Given the central role of Trop-2 in the modulation of E-cadherin [9] and Akt [3] function, we hypothesized that CD9 may act as an active scaffold of a Trop-2-centered membrane super-complex. Hence, we carried out a dynamic protein–protein interaction assay based on tripartite split GFP [50], whereby the GFP β-strand 10 (GFP10) or β-strand 11 (GFP11) were fused to the CD9 C- or N-terminal tail, respectively, and GFP10 or GFP11 tags were fused to the Trop-2 C-terminal tail (Fig. 4E). Green fluorescence reconstituted from GFP10, GFP11 and the freely diffused GFP β-strands 1-9 (GFP1-9) was observed at the cell membrane when GFP11 was fused to the CD9 C-terminal tail in HT-29 cells (Fig. 4E, left). No cell membrane green fluorescence was detected when the GFP10 tag was fused to the CD9 N-terminal tail (Fig. 4E, right), due to insufficient proximity of the GFP segments. Hence, the C-terminal tail of CD9 is a close interactor of the Trop-2 cytoplasmic tail.

Binding of CD9 to Trop-2 was validated by co-immunoprecipitation with Trop-2 from KM12SM transfectant lysates (Fig. 4F). The Trop-2/CD9 binding was abolished by deleting the Trop-2 HIKE motif or by replacing HIKE with seven Gly residues, as a co-linear substitute of HIKE (Fig. 4F). Previous evidence had indicated that the C-terminal tail of CD9 plays a critical role in the assembly and function of the tetraspanin webs [51]. Our findings showed that the C-terminal tail of CD9 is involved in the physical interaction with Trop-2, and that HIKE is the CD9 docking site on the Trop-2 cytoplasmic tail. Our findings showing that the Trop-2_ΔHIKE mutant is able to transduce $Ca^{2+}$ signaling (Fig. 2F) suggested that CD9 might act downstream of this Trop-2 function, for modulating the assembly of the signaling super-complex. We obtained suppression of CD9 expression by Crispr/Cas9 in KM12SM/Trop-2 transfectants (see below). Time-lapse confocal microscopy revealed that stimulation with the 162-46.2 mAb leads to rise of intracellular $Ca^{2+}$ in the absence of CD9 expression (Supplementary Fig. S1B), confirming that CD9 acts downstream of the $Ca^{2+}$ signal transduction function of Trop-2 to drive formation and activity of the signaling super-complex.

The association of CD9 with PKCα [48] suggested that CD9 may mediate cognate binding of PKCα to Trop-2, for subsequent phosphorylation at Ser303. Consistent with this, Trop-2 was shown to co-recruit CD9 and PKCα to the cell membrane (Supplementary Fig. S5A), over extensive regions of the cell membrane (Supplementary Fig. S5B). Trop-2–driven membrane co-recruitment of CD9 and PKCα was quantitatively validated by cell-surface protein biotinylation followed by streptavidin-agarose pull-down and Western blotting analysis (Fig. 4G). The dynamics of CD9 and PKCα co-recruitment to the cell membrane were assessed. We categorized the distribution of CD9 and PKCα along the cell perimeter in five localization classes, and scored their distribution profiles (Supplementary Fig. S5D). CD9/PKCα co-localization was barely detectable in Trop-2–null cells. Trop-2 expression stimulated membrane localization of CD9 and PKCα (Supplementary Fig. S5D and Supplementary Table S1E). Next, we used PMA, which induces intracellular $Ca^{2+}$ rise (Supplementary Fig. S5C), to assess PKCα and CD9 co-distribution at the cell membrane. Tight correlation shown by high Spearman rho coefficients for P-PKCα and CD9 membrane levels ($P = 0.001–0.005$) was seen all along the five membrane localization classes, which supports a tight functional interaction between PKCα and CD9 upon activation by Trop-2 and PMA (Fig. 2B, Supplementary Fig. S5E, F and Supplementary Table S1E).

## CD9 is an obligate mediator of the Trop-2 cancer growth signaling network

Inhibition of CD9 expression was obtained in KM12SM (Fig. 5A, B) and in HT-29 (Fig. 5F) cells by Crispr/Cas9. This resulted in a significant reduction of KM12SM/Trop-2 growth, but did not affect the growth of KM12SM/vector cells (Fig. 5C). Using a 3D sphere-forming assay in vitro, we showed that the growth of

KM12SM/Trop-2 spheroids was compromised upon CD9 inhibition, while the growth of KM12SM/vector spheroids was unaffected (Fig. 5D). Consistent with a required role of CD9 in the Trop-2 signaling, inhibition of CD9 was found to abrogate the Trop-2-induced cleavage of E-cadherin (Fig. 5A), which we recently demonstrated to mediate the pro-invasive capabilities of Trop-2 [9].

Our findings had indicated a pivotal role of Trop-2 on regulation of cytoskeletal dynamics. Treatment of CRC cells with cytochalasin D was shown to induce loss of recruitment of CD9 to the cell membrane (Supplementary Fig. S4G). Thus, a bidirectional relationship takes place between Trop-2 and cytoskeletal components to drive the assembly and function of the Trop-2-driven signaling super-complex.

We then asked whether the Trop-2/CD9 complex was required for the capacity of CRC cells to invade extracellular matrices. Matrigel invasion of KM12SM cells ± Trop-2 transfectants, upon Crispr/Cas9 knockout of the *CD9* gene, was followed by 3D imaging of live cells stained with calcein-AM at 7 days after seeding on the porous membrane of a transwell. Confocal microscopy analysis of Z-stacked pictures showed that only Trop-2-positive cells where CD9 was also expressed were able to invade the matrix (Fig. 5E). The effect of CD9 suppression on the Trop-2-dependent cleavage of E-cadherin and on the invasive

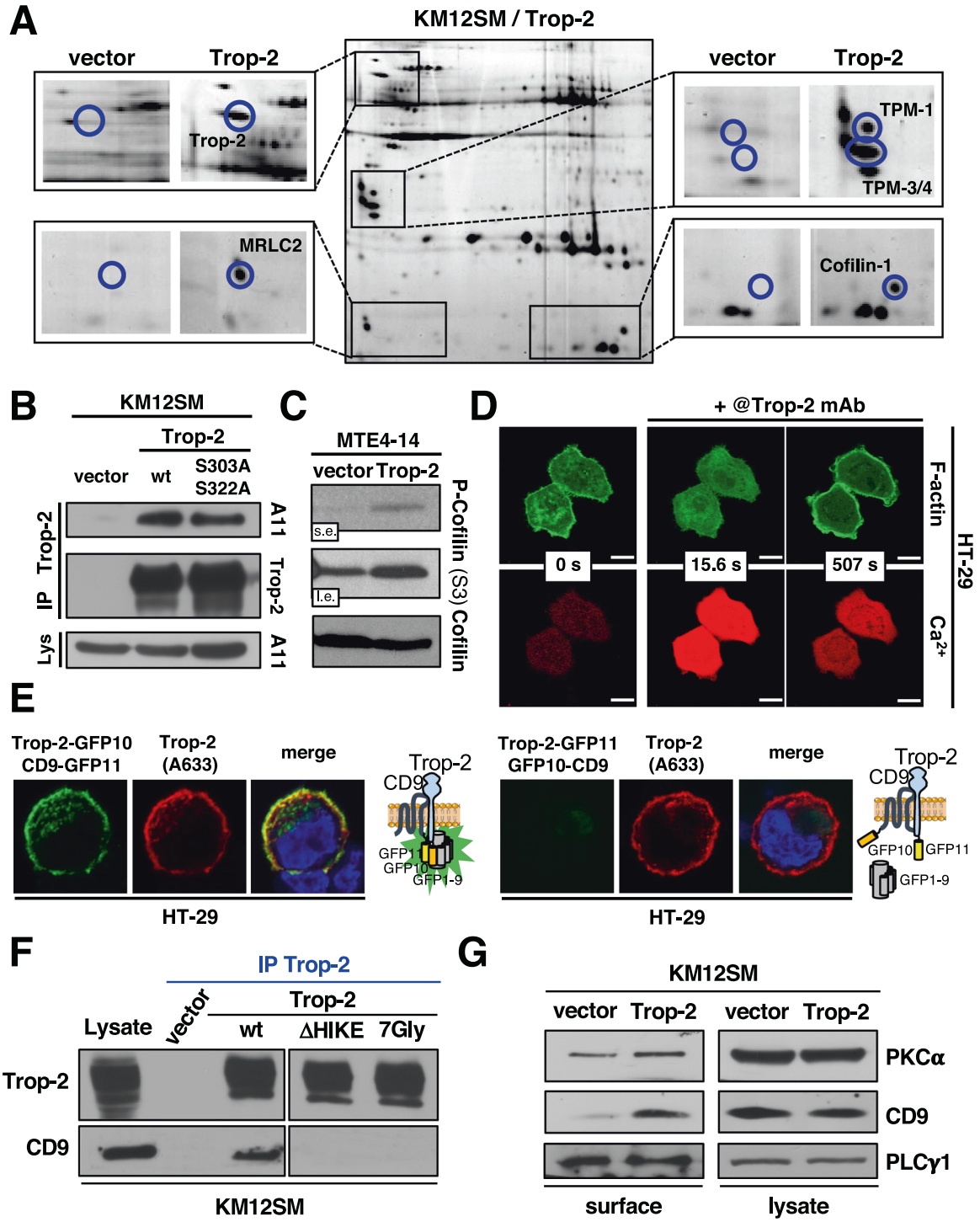

**Fig. 4 Trop-2 modulates cytoskeletal dynamics and interacts with CD9 at the cell membrane. A** 2D-PAGE analysis showing silver-stained Trop-2 immunoprecipated material from KM12SM/Trop-2 cells (center). KM12SM/vector and KM12SM/Trop-2 cells were subjected to immunoprecitations with the T16 anti-Trop-2 mAb. Co-immunoprecipitated proteins were identified by 2D PAGE/MS–MS. Magnification boxes show comparisons between immunoprecipitates from KM12SM/vector (left) and KM12SM/Trop-2 (right). The protein spots isolated from the Trop-2 co-immunoprecipitated material and subjected to MS–MS analysis are as follows: Trop-2 benchmark (upper left panel); MRLC2 (lower left panel); tropomyosins (upper right panel); cofilin-1 (lower right panel). The full list is presented in Table S1A. **B** Western blotting analysis of annexin A11 co-immunoprecipitated with Trop-2 from KM12SM cells transfected with wtTrop-2 and with the Trop-2_S303A-S322A mutant. **C** Western blotting analysis of P-cofilin (Ser-3) in MTE4-14/vector and MTE4-14/Trop-2 transfectants. S.e., short exposure. L.e., long exposure. Total cofilin, control of protein loading. **D** Fluorescence confocal microscopy of HT-29 cells transfected with Lifeact-GFP (green) and CMV-R-GECO1.2 (red), upon cross-linking of Trop-2 with the 162-46.2 mAb. Time frames at 15.6 and 507 s show the depolymerization/repolymerization cycles of the cortical actin. Scale bars, 10 μm. **E** *Left* HT-29 transfected with soluble GFP1-9, CD9-GFP11 (GFP11 fused to the CD9 C-terminal tail) and Trop-2-GFP10 (GFP10 fused to the Trop-2 C-terminal tail). Reconstitution of the green fluorescence resulting from physical binding of Trop-2 and CD9 is shown. **E** *Right* HT-29 transfected with soluble GFP1-9, GFP10-CD9 (GFP10 tag fused to the CD9 N-terminal tail) and Trop-2-GFP11 (GFP11 tag fused to the Trop-2 C-terminal tail). No cell membrane green fluorescence was detected, due to insufficient proximity of the GFP segments. Red signal, expression of endogenous Trop-2, of Trop-2-GFP10, and of Trop-2-GFP11 as detected by the T16 mAb. **F** Western blotting analysis of Trop-2 (top) and CD9 (bottom) on Trop-2 immunoprecipitates from KM12SM cells transfected with empty vector, wt Trop-2, Trop-2_ΔHIKE, and Trop-2_HIKE-7Gly. Lys: protein lysate from KM12SM/Trop-2 cells. **G** Western blotting analysis of PKCα and CD9 levels at the cell membrane (CD9) or associated to membrane proteins (PKCα), as obtained by surface protein biotinylation followed by pull-down with streptavidin-agarose (left). Corresponding levels in the total cell lysates are also shown (right). PLCγ1 was used as control of protein loading.

capabilities of human CRC cells was further confirmed in HT-29 (Fig. 5F, G), supporting the high impact of these findings in human CRC development and progression.

The assembly of the Trop-2-driven membrane super-complex was then investigated in vivo, by assessing the interaction between Trop-2 and CD9 in KM12SM/vector and KM12SM/Trop-2 transfectants grown as xenotransplants in immunosuppressed mice (Fig. 6A). Western blotting analysis of Trop-2 immunoprecipitates obtained from corresponding tumor samples was performed, and showed that the Trop-2/CD9 interaction takes place in vivo (Fig. 6B).

## NGS analysis of the Trop-2 super-complex in CRC models

We assessed the expression of Trop-2, $Na^+/K^+$-ATPase, CD9, PKCα, cofilin-1 across normal tissues and tumor types (Supplementary Table S2; www.proteinatlas.org). Expression analysis of these proteins in normal vs. cancer tissues showed that all of the components of the super-complex were broadly expressed in normal tissues and by most cancer types. However, an exception was represented by the colon mucosa, where the expression of Trop-2 was undetectable in normal tissue as compared with $Na^+/K^+$-ATPase, CD9, PKCα, cofilin-1 (Supplementary Table S2A vs. Supplementary Tables S2B–E). In the corresponding transformed colon tissues, Trop-2 expression was strongly up-regulated (Supplementary Table S2A and below), suggesting a role of this molecule as a trigger of the signaling super-complex.

Trop-2 was shown not to affect the absolute expression levels of $Na^+/K^+$-ATPase, CD9, PKCα, cofilin-1 (Figs. 1E, 4C, 5A, B). On the other hand, it did induce phosphorylation of PKCα and cofilin-1 (Figs. 2C, 3A, D, 4C). Thus, a signaling model is suggested whereby an endogenous, broadly expressed $Na^+,K^+$-ATPase/CD9/PKCα/cofilin-1 super-complex is dormant in Trop-2–null cells and is triggered by Trop-2 to override basal cell growth and to acquire malignant features (Fig. 6C).

The expression of the effectors of this Trop-2 signaling module was investigated by NGS analysis of individual KM12SM xenotransplant transcriptomes (Supplementary Table S3). Our model predicted that all key components of the Trop-2 module: (i) should be expressed by tumor cells; (ii) should be highly correlated across individual tumor samples in each experimental subgroup, as well as across subgroups. Intra-group analysis was performed, and revealed extremely high R correlation coefficients, and reproducible mRNA sequence profiles across independent primary tumors (Supplementary Table S3). Averaged intra-group profiles were then used for comparisons of the growth-associated parameters in Trop-2 tumors vs. controls. This showed correlated expression of all components of the Trop-2 module, with extremely high significance ($P \approx 0$) and correlation coefficients (CD9, PKCα, $Na^+/K^+$-ATPase, >0.99). Expressed sequence tag profiles of individual parameters were strongly conserved, with high correlation of all-parameter profiles in control vs. Trop-2 tumors ($R = 0.9817$; $P = 0$) (Supplementary Table S3F). Thus, all key components of the Trop-2 super-complex are coordinatively expressed across individual tumors and tumor subgroups in vivo.

## The Trop-2-super-complex determines disease outcome in patients with CRC

We investigated whether our signaling model held true in primary human CRC. To validate our model, we assessed whether the expression of the components of the Trop-2 dynamic super-complex had impact on cancer prognosis. We then went on to determine whether a correlated expression had stronger impact than individual determinants alone.

In silico analysis of expression profiles in a test case series ($N = 160$) of stage II-III CRC (DNA-microarray dataset, GSE24551 [52]) revealed that the joint expression of Trop-2, $Na^+/K^+$-ATPase, CD9, PKCα, and cofilin-1 had heavy prognostic impact, with a hazard ratio (HR) for death of 7.36 ($P = 0.0012$). The $Na^+,K^+$-ATPase/CD9/PKCα/cofilin-1 complex alone, i.e., in the absence of Trop-2, had no measurable impact ($P = 0.163$), supporting a model of Trop-2 activation of a dormant, ubiquitously expressed signaling super-complex as pivotal to cancer malignant progression.

Assessment of HRs of each individual prognostic determinant or combination of them in presence vs. absence of Trop-2 expression was systematically carried out. Survival analysis of disease progression showed no significant impact of $Na^+/K^+$-ATPase, PKCα, cofilin-1. This was barely reached by CD9 only (HR = 2.45; $P = 0.026$). The impact of Trop-2 alone on CRC survival had the highest significance level ($P = 0.00058$) (Fig. 7A and Supplementary Table S4A). Most remarkably, though, joint determination of Trop-2 with each super-complex component through correlated analyses reproducibly shifted impact to sharply more severe disease outcome in all cases (Fig. 7A, red plots).

Parallel findings were obtained by analysis of an independent validation case series ($N = 95$) of CRC patients (DNA-microarray dataset, GSE30378 [53]) supporting a Trop-2-driven super-complex model (Supplementary Table S4, panel ii).

Trop-2 and CD9 expression at protein level was investigated by IHC in a case series of patients with CRC ($N = 177$). Only CRC patients who did not show any pathological evidence of nodal involvement and distant metastasis, and who did not receive adjuvant systemic therapy were included in the study (Supplementary Table S4B, panel i). High CD9 expression was shown to correlate with the occurrence of tumor relapse ($p = 0.010$)

(Supplementary Table S4B, panel ii). Correlation analysis further revealed that CD9 positively correlates with membrane Trop-2 (Spearman $\rho = 0.202$; two-tailed $P = 0.007$), consistent with functional interactions between membrane/active form of Trop-2 [54] and CD9 (Supplementary Table S4B, panel iii).

High expression of Trop-2 and CD9 was observed in moderately and poorly differentiated CRC tissues, whereas both proteins were expressed at low levels in well differentiated tissues (Fig. 7B). Consistent with this, biparametric Trop-2/CD9 analysis of CRC was found to discriminate subgroups where patients with high expression of Trop-2 and CD9 (Fig. 7C, red curve) showed significantly higher risk of metastatic relapse (HR = 4.1; C.I. = 1.19–14.15; $p = 0.026$) than patients with low expression of both proteins (Fig. 7C, black curve).

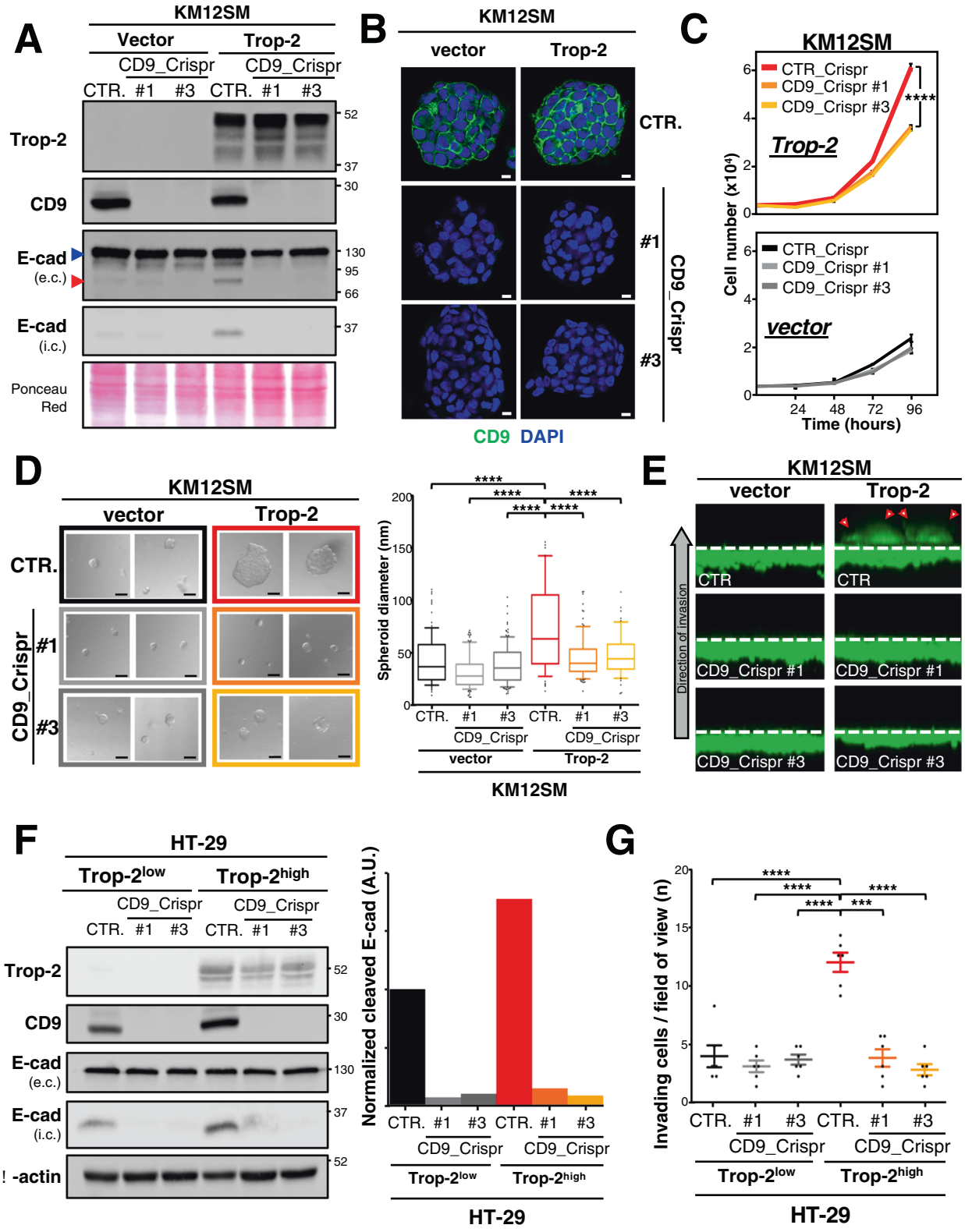

**Fig. 5 CD9 is an obligate mediator of Trop-2 signaling. A** Western blotting analysis of Trop-2 and CD9 expression (top panels), and of E-cadherin proteolytic cleavage (bottom panels) in KM12SM/vector (left) and KM12SM/Trop-2 (right) transfectants upon Crispr/Cas9-mediated knockout of CD9. Crispr #1 and #3 represent two sgRNAs targeting two different regions of the CD9 gene. E-cadherin cleavage was detected with an Ab targeting the extracellular portion of the molecule (third panel from top) and with an Ab targeting the intracellular domain of E-cadherin (fourth panel from top). CTR, ineffective sgRNAs. Ponceau Red staining, control of protein loading. **B** Fluorescence confocal microscopy representative images showing CD9 (green) expression in KM12SM/vector (left) and KM12SM/Trop-2 (right) transfectants upon Crispr/Cas9 knockout of CD9 (Crispr #1 and #3). CTR, ineffective sgRNA. DAPI (blue), nuclei counterstaining. Scale bars, 10 μm. **C** Growth curves of KM12SM/vector (left) and KM12SM/Trop-2 (right) transfectants upon Crispr/Cas9 knockout of the CD9 gene. Bars, SD. $^{****}P < 0.0001$ (KM12SM/Trop-2 + control CRISPR vs. other groups). **D** Matrigel spheroid-forming assay of KM12SM/Trop-2 (top) and KM12SM/vector (bottom) upon Crispr/Cas9 knockout of CD9. Longest spheroid diameters were calculated after 7 days in culture. Comparison among groups is shown in the box and whisker plot, where boxes extend from the 25$^{th}$ to the 75$^{th}$ percentile, and whiskers are drawn down to the 10$^{th}$ percentile and up to the 90$^{th}$ percentile (right panel). $^{****}P < 0.0001$ (KM12SM/Trop-2 + control CRISPR vs. other groups). **E** Inverse Matrigel invasion of KM12SM/vector (left) and KM12SM/Trop-2 (right) transfectants transfectants upon Crispr/Cas9 knockout of CD9. Dashed lines indicate the porous membrane of the transwell filter where the cells were seeded at time = 0. Arrowheads, cells that penetrated the Matrigel matrix through the porous membrane. Green fluorescent cells result from live-cell staining with calcein-AM. The grey arrow indicates the direction of cell migration during the process of Matrigel invasion. **F** *Left* Western blotting analysis of the levels of Trop-2, CD9, full-length, and cleaved E-cadherin in HT-29/Trop-2$^{low}$ and HT-29/Trop-2$^{high}$ cells upon knockout of CD9 expression obtained using Crispr #1 and #3 sgRNAs. CTR, ineffective sgRNAs. Levels of β-actin were used as control of protein loading. **F** *Right* Assessment of E-cadherin cleavage obtained from quantification of the corresponding western blotting bands of cleaved E-cadherin, normalized by the loading control, β-actin. **G** Inverse Matrigel invasion of HT-29/Trop-2$^{low}$ and HT-29/Trop-2$^{high}$ cells upon Crispr/Cas9 knockout of CD9. The experiment was repeated two times, and three random areas of the filter were acquired each time for evaluation. Cells that penetrated the Matrigel matrix were counted and comparison of the means ± SEM among groups is shown in the bar plot. $^{***}P = 0.001$; $^{****}P < 0.0001$.

## DISCUSSION

The transmembrane glycoprotein Trop-2 is a key driver of cancer progression [2, 6, 9, 55]. Our findings show here that Trop-2 acts by activating a ubiquitously expressed, functionally dormant, super-complex, which signals through dynamic interactions of its components at the cell membrane. This activated complex then leads cancer cells to acquire malignant properties in vitro as well as in vivo.

Our findings show that Trop-2 binds membrane $Na^+/K^+$-ATPase, and induces the release of $Ca^{2+}$ from the endoplasmic reticulum through IP3Rs localized at junctional $Ca^{2+}$ signaling microdomains [19]. This event catalizes mTORC2-dependent membrane translocation of active PKCα [4, 56]. Inhibition of mTORC2 was shown to lead to reduced growth of Trop-2-expressing cells. Translocation of primed PKCs to the plasma membrane leads to PKC binding to tetraspanin proteins, among them CD9, which brings PKCs in proximity of their kinase substrates, such as $\beta_1$ integrins [48] and EGFR [57]. We previously showed that Trop-2 binds $\beta_1$ integrins and modulates their bidirectional signaling in prostate cancer, by inducing dynamic assembly and disassembly of integrin adhesions via talin and FAK [4, 38, 39]. CD9 was earlier demonstrated to modulate breast cancer cell motility by guiding talin localization in focal adhesions [58]. Consistent with this, our data here showed that: (a) Trop-2 promotes localization of CD9 at membrane sites where it recruits primed, $Ca^{2+}$–bound PKCα; (b) CD9 is an obligate hub of Trop-2-driven signaling; (c) inhibition of CD9 does not affect the Trop-2 $Ca^{2+}$ transduction; (d) inhibition of CD9 prevents Trop-2 from overriding the basal growth program of tumor cells and from activating the cleavage of E-cadherin, which is required for malignant progression of CRC [9]. These data provide a key advancement of the knowledge of the mechanisms that underlie cancer cell relationships with the tumor microenvironment (TME), where CD9 appears to be a central organizer upon activation by Trop-2. As both CD9 and Trop-2 are recruited to extracellular vesicles [38, 59, 60], future studies will define how the Trop-2-dependent signaling super-complex will affect the cancer-TME relationships through modulation of exosome biogenesis and secretion.

Targeted mutagenesis of the Trop-2 cytoplasmic tail showed that the Ser303-encompassing HIKE region [32, 33, 61] is a key docking site for PKCα at the plasma membrane, as deletion of HIKE preserved the Trop-2 $Ca^{2+}$ transducing activity, but prevented Trop-2 from recruiting PKCα. This led us to propose the existence of a feed-forward signaling in cancer cells where Trop-2 transduces the $Ca^{2+}$ signals required for PKCα to translocate to the cell membrane, where it phosphorylates the Trop-2 cytoplasmic tail. A two-pronged phosphorylation of the Trop-2 cytoplasmic tail at Ser303 and Ser322 was shown to be required to fully activate Trop-2 to transmit growth signals mediated by Akt, ERK, NFkB, and cyclin D1 [1–3], via remodeling of the β-actin/α-actinin/myosin II cytoskeleton by gelsolin, cofilin-1, annexins A1/A6/A11. Mori et al. showed that Trop-2 is phosphorylated at Ser322 by PKCα and PKCδ in CRC cells [30], and that Ser322 phosphorylation regulated cell–cell junctions and cell motility, but no impact on proliferation rates was detected. Our observations increase the sensitivity of the assays by Mori et al. and demonstrate the Trop-2/PKCα feed-forward activatory signaling further spurs tumor growth and malignant progression.

Whole transcriptome profiling of preclinical human tumor models revealed that all the key components of the Trop-2 super-complex are coordinately transcribed. Coregulated expression of the components of this Trop-2 module was expected to facilitate the assembly of signaling super-complexes for driving disease progression. This hypothesis was shown to hold true in human CRC progression. Analysis at both RNA and protein levels demonstrated that the Trop-2–centered super-complex had a strong clinical impact on the survival of patients with CRC. Correlated expression of all Trop-2 super-complex components was shown to have a stronger prognostic impact than any individual parameter per se, with higher risk of cancer relapse and patient death. Of interest, PKCα alone showed no significant impact on the prognosis of patients with CRC. However, PKCα worsened negative disease outcomes when coexpressed with the other super-complex components. This may help explaining previous conflicting findings on PKCα function in tumors [62] and suggests that Trop-2 may represent a novel predictive marker of tumor responses to PKCα inhibitors. We wish to note that drug screening and expression modulation revealed that inhibition of $Ca^{2+}$ signaling, of CD9 or PKCα expression, of β-actin polymerization diminished growth of Trop-2–expressing cancer cells, but had no effect on the growth of Trop-2–null cells. Trop-2 has recently emerged as a target of anti-Trop-2 antibodies [11, 12]. Knowledge on pivotal nodes of Trop-2 signaling may pave the way for the development of novel therapeutic approaches, based on the parallel assessment of Trop-2- driven super-complex components.

## MATERIALS AND METHODS

### CRISPR/Cas9

sgRNAs targeting the *CD9* gene were designed using the Zhang laboratory CRISPR design tools (http://www.genome-engineering.org) and cloned into the plasmid LentiCRISPRv2 (Addgene #52961) [63]. Lentiviruses were

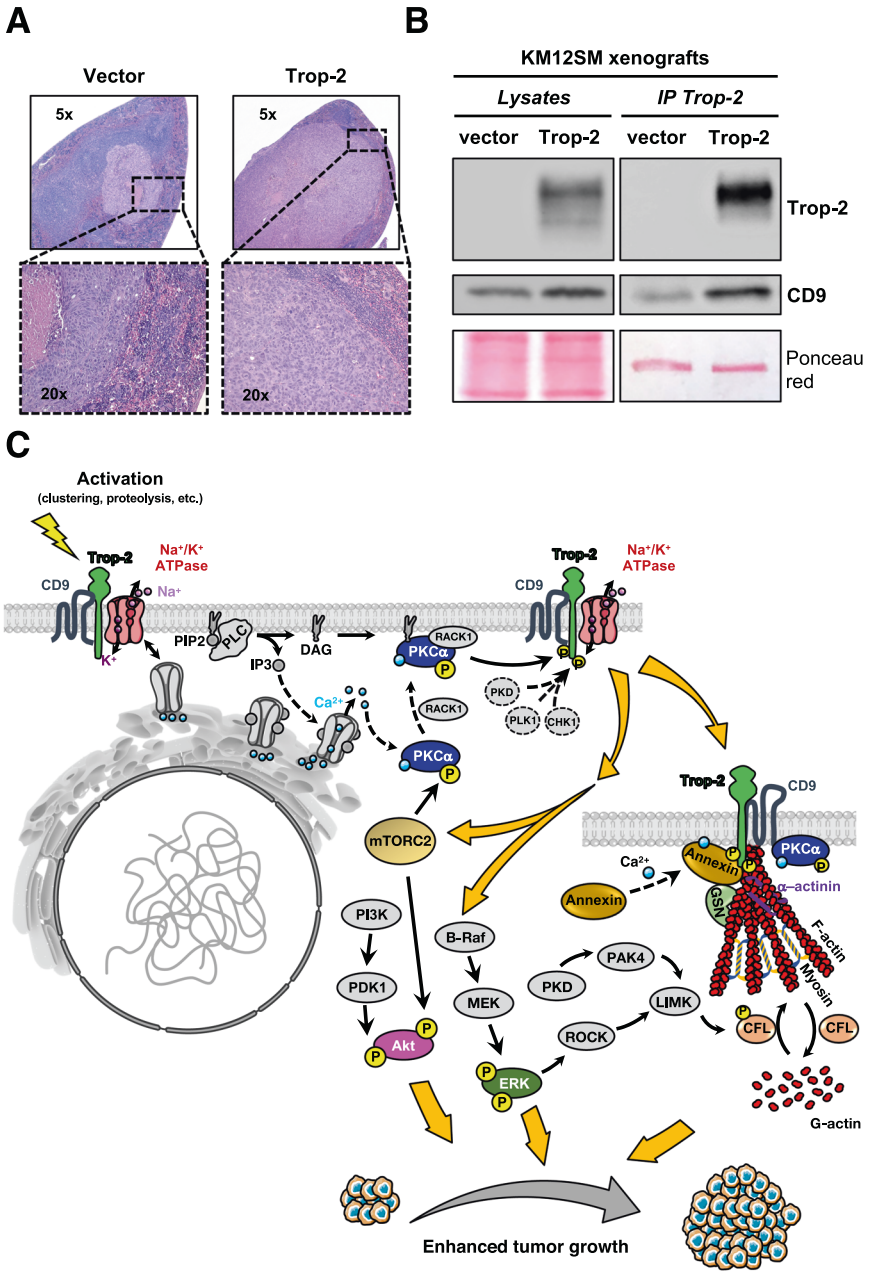


**Fig. 6 The Trop-2-centered growth control module. A** Intrasplenic tumor growth of KM12SM/vector ($n = 37$) and KM12SM/Trop-2 ($n = 31$) transfectants in immunosuppressed mice. Representative hematoxylin and eosin tissue staining is shown. The detailed analysis is shown in Guerra et al. [9]. **B** KM12SM/vector ($n = 4$) and KM12SM/Trop-2 ($n = 5$) spleen xenotransplants whose major and minor diameters were both ≥5 mm [9] were pulled and lysed in Brij-97 buffer to preserve tetraspanin-mediated interactions, and Trop-2 was immunoprecipitated using the T16 mAb. Western blotting analysis shows Trop-2 (top) and CD9 (bottom) expression in tumor lysates (left panel) and in the Trop-2 immunoprecipitates (right panel). Ponceau Red staining, control of protein loading. The Ponceau Red staining on the right shows the levels of the whole IgGs used for the immunoprecipitation experiment, and represents a protein loading control. **C** Schematic representation of the Trop-2 signaling at the cell membrane and the corresponding downstream effector cascade. Activation of Trop-2 at the cell membrane (via clustering, proteolytic cleavage or other yet unidentified mechanisms) triggers intracellular release of $Ca^{2+}$ predominantly from intracellular stores through the interaction with CD9 and $Na^{+}/K^{+}$-ATPase. This drives translocation of pre-activated/mTORC2-phosphorylated PKCα at the cell membrane for full activation. Activated PKCα binds and phosphorylates the Trop-2 cytoplasmic tail at Ser303 through a bridging function carried out by CD9. This is accompanied by phosphorylation of Ser322 by other, as yet unidentified, kinases. These events activate Trop-2 to induce downstream effectors, such as Akt and ERK. $Ca^{2+}$ induces membrane translocation of Annexins, which mediate Trop-2 binding to cortical F-actin. Trop-2 stimulates cytoskeletal dynamics by regulating the actin severing function of cofilin, through PAK4 and LIMK, gelsolin, α-actinin and myosin II, for tumor growth and malignant progression. Findings from earlier literature are shown in grayscale, while all novel findings from this study are shown as colored illustrations.

produced in HEK293T cells by co-transfection of LentiCRISPRv2-sgRNA with the packaging plasmids pVSVg (Addgene #8454) and psPAX2 (Addgene #12260), purified from the supernatant and utilized for infection of the target cells. Stable functional knockout of *CD9* were selected in puromycin 3 μg/ml.

## Cell growth assays

Cell transfectants were seeded at 1500–3000 cells/well in 96-well plates (five replica wells per data point). Cell growth was quantified by staining with crystal violet [1], upon normalization against standard cell reference

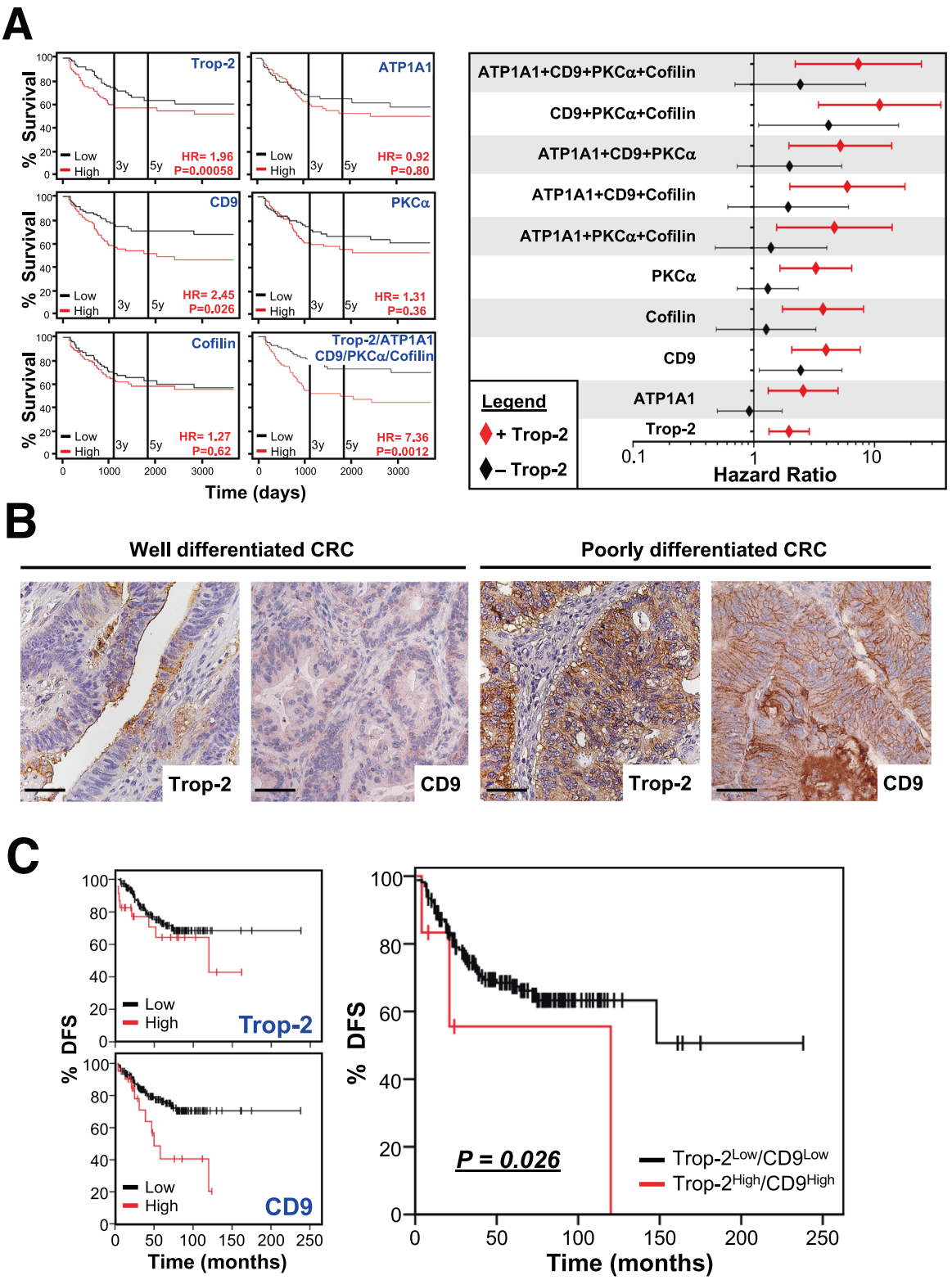


**Fig. 7 Expression of the Trop-2-driven super-complex correlates with the clinical outcome of patients with CRC. A** *Left* Kaplan–Meier plots showing impact of the Trop-2-centered super-complex (individual determinants vs. combinations) on the overall survival of patients with CRC. Parallel assessment of super-complex parameters is presented in Table S4A. **A** *Right* Forest plot of the differential impact of individual determinants of the growth module vs. combinations of them on the overall survival of patients with CRC. Red bars, combinations of markers including the contribution of Trop-2. Black bars, combinations of markers excluding the contribution of Trop-2. **B** IHC analysis of Trop-2 and CD9 expression in tissue samples from poorly differentiated (left) and well differentiated (right) human CRC. Scale bars, 50 μm. **C** Kaplan–Meier plots showing the impact of Trop-2 and CD9 expression either as individual determinants (left) or in combination (right) on disease-free survival (DFS) of patients with CRC. Low and high protein levels were determined by IHC analysis.

curves of twofold serially diluted cell samples. 3D sphere-forming assays were performed as described [64].

### Invasion assay

Inverse Matrigel invasion assays were performed as described [65]. 3D reconstruction of invading cells was carried out by confocal microscopy using a 20× objective and optical Z-sections at 15 µm intervals for image acquisition.

### Calcium imaging

Intracellular $Ca^{2+}$ levels were monitored as described [66]. Fluorescence images were acquired at 5 frames/s and processed with Metafluor (Molecular Device, Sunnyvale, CA, USA). Mean fluorescence intensity was calculated as f/f0, where f is the fluorescence emission of a single loaded cell acquired during the time lapse, and f0 is the mean fluorescence intensity of the same cell before signaling activation.

### Immunohistochemistry

Samples were fixed in PBS-buffered formalin, pH 7.2, embedded in paraffin and processed as described [6]. Blinded scoring of tissue slides were performed by two independent observers (RL, MP). Where indicated, staining intensity was categorized in four classes: negative (no staining), 1 (weak), 2 (moderate), and 3 (strong).

### Transcriptomics and NGS

Tumor samples were flash frozen after collection and stored at −80 °C. Samples were processed and sequenced using an Illumina Hiseq 1000, following manufacturer' indications.

### Statistical analysis

Normality of measurement distribution was verified with the Wilk–Shapiro normality test (www.graphpad.com). Spearman nonparametric correlation coefficients were computed for protein expression levels in human cancer samples. Relationship between Trop-2 expression and clinical-pathological parameters was assessed by Pearson's $\chi^2$ and Fisher's exact test. ANOVA and post hoc Bonferroni's *t* test were used for comparison of cell growth curves. No statistical method was used to predetermine the sample size.

Details on experimental procedures are provided in Supplementary Materials and Methods.

## REFERENCES

1. Guerra E, Trerotola M, Aloisi AL, Tripaldi R, Vacca G, La Sorda R, et al. The Trop-2 signalling network in cancer growth. Oncogene. 2013;32:1594–600.
2. Trerotola M, Cantanelli P, Guerra E, Tripaldi R, Aloisi AL, Bonasera V, et al. Up-regulation of Trop-2 quantitatively stimulates human cancer growth. Oncogene. 2013;32:222–33.
3. Guerra E, Trerotola M, Tripaldi R, Aloisi AL, Simeone P, Sacchetti A, et al. Trop-2 induces tumor growth through Akt and determines sensitivity to Akt inhibitors. Clin Cancer Res. 2016;22:4197–205.
4. Trerotola M, Li J, Alberti S, Languino LR. Trop-2 inhibits prostate cancer cell adhesion to fibronectin through the β1 integrin-RACK1 axis. J Cell Physiol. 2012;227:3670–7.
5. Guerra E, Trerotola M, Dell' Arciprete R, Bonasera V, Palombo B, El-Sewedy T, et al. A bi-cistronic CYCLIN D1-TROP2 mRNA chimera demonstrates a novel oncogenic mechanism in human cancer. Cancer Res. 2008;68:8113–21.
6. Trerotola M, Guerra E, Ali Z, Aloisi AL, Ceci M, Simeone P, et al. Trop-2 cleavage by ADAM10 is an activator switch for cancer growth and metastasis. Neoplasia. 2021;23:415–28.
7. Rios-Doria J, Day KC, Kuefer R, Rashid MG, Chinnaiyan AM, Rubin MA, et al. The role of calpain in the proteolytic cleavage of E-cadherin in prostate and mammary epithelial cells. J Biol Chem. 2003;278:1372–9.
8. Maretzky T, Reiss K, Ludwig A, Buchholz J, Scholz F, Proksch E, et al. ADAM10 mediates E-cadherin shedding and regulates epithelial cell-cell adhesion, migration, and beta-catenin translocation. Proc Natl Acad Sci USA. 2005;102:9182–7.
9. Guerra E, Trerotola M, Relli V, Lattanzio R, Tripaldi R, Vacca G, et al. Trop-2 induces ADAM10-mediated cleavage of E-cadherin and drives EMT-less metastasis in colon cancer. Neoplasia. 2021;23:898–911.
10. Ripani E, Sacchetti A, Corda D, Alberti S. The human Trop-2 is a tumor-associated calcium signal transducer. Int J Cancer. 1998;76:671–6.
11. Thomas A, Pommier Y. Targeting topoisomerase I in the era of precision medicine. Clin Cancer Res. 2019;25:6581–9.
12. Bardia A, Mayer IA, Vahdat LT, Tolaney SM, Isakoff SJ, Diamond JR, et al. Sacituzumab govitecan-hziy in refractory metastatic triple-negative breast cancer. N Engl J Med. 2019;380:741–51.
13. Fornaro M, Dell'Arciprete R, Stella M, Bucci C, Nutini M, Capri MG, et al. Cloning of the gene encoding TROP-2, a cell-surface glycoprotein expressed by human carcinomas. Int J Cancer. 1995;62:610–8.
14. El Sewedy T, Fornaro M, Alberti S. Cloning of the murine *Trop2* gene: conservation of a PIP2-binding sequence in the cytoplasmic domain of Trop-2. Int J Cancer. 1998;75:324–30.
15. Alberti S, Miotti S, Stella M, Klein CE, Fornaro M, Ménard S, et al. Biochemical characterization of Trop-2, a cell surface molecule expressed by human carcinomas: formal proof that the monoclonal antibodies T16 and MOv-16 recognize Trop-2. Hybridoma. 1992;11:539–5.
16. Moore EDW, Etter EF, Philipson KD, Carrington WA, Fogarty KE, Lifshitz LM, et al. Coupling of the Na+/Ca2+exchanger, Na+/K+ pump and sarcoplasmic reticulum in smooth muscle. Nature. 1993;365:657–60.
17. Liang M, Tian J, Liu L, Pierre S, Liu J, Shapiro J, et al. Identification of a Pool of Non-pumping Na/K-ATPase. J Biol Chem. 2007;282:10585–93.
18. Tian J, Cai T, Yuan Z, Wang H, Liu L, Haas M, et al. Binding of Src to Na+/K+-ATPase forms a functional signaling complex. Mol Biol Cell. 2005;17:317–26.
19. Tian J, Xie ZJ. The Na-K-ATPase and calcium-signaling microdomains. Physiology. 2008;23:205–11.
20. Matchkov VV, Krivoi II. Specialized functional diversity and interactions of the Na, K-ATPase. Front Physiol. 2016;7:179.
21. Haas M, Wang H, Tian J, Xie Z. Src-mediated inter-receptor cross-talk between the Na+/K+-ATPase and the epidermal growth factor receptor relays the signal from ouabain to mitogen-activated protein kinases. J Biol Chem. 2002;277:18694–702.
22. Shen J-J, Zhan Y-C, Li H-Y, Wang Z. Ouabain impairs cancer metabolism and activates AMPK-Src signaling pathway in human cancer cell lines. Acta Pharmacol Sin. 2020;41:110–8.
23. Chen D, Song M, Mohamad O, Yu SP. Inhibition of Na+/K+-ATPase induces hybrid cell death and enhanced sensitivity to chemotherapy in human glioblastoma cells. BMC Cancer. 2014;14:716.
24. Tian J, Li X, Liang M, Liu L, Xie JX, Ye Q, et al. Changes in sodium pump expression dictate the effects of ouabain on cell growth. J Biol Chem. 2009;284:14921–9.
25. Ninsontia C, Chanvorachote P. Ouabain mediates integrin switch in human lung cancer cells. Anticancer Res. 2014;34:5495.
26. Larre I, Lazaro A, Contreras RG, Balda MS, Matter K, Flores-Maldonado C, et al. Ouabain modulates epithelial cell tight junction. Proc Natl Acad Sci. 2010;107:11387.
27. Morikawa K, Walker SM, Nakajima M, Pathak S, Jessup JM, Fidler IJ. Influence of organ environment on the growth, selection, and metastasis of human colon carcinoma cells in nude mice. Cancer Res. 1988;48:6863–71.
28. Basu A, Goldenberg DM, Stein R. The epithelial/carcinoma antigen EGP-1, recognized by monoclonal antibody RS7-3G11, is phosphorylated on serine 303. Int J Cancer. 1995;62:472–9.
29. Wanger TM, Dewitt S, Collins A, Maitland NJ, Poghosyan Z, Knauper V. Differential regulation of TROP2 release by PKC isoforms through vesicles and ADAM17. Cell Signal. 2015;27:1325–35.
30. Mori Y, Akita K, Ojima K, Iwamoto S, Yamashita T, Morii E, et al. Trophoblast cell surface antigen 2 (Trop-2) phosphorylation by protein kinase C alpha/delta (PKCalpha/delta) enhances cell motility. J Biol Chem. 2019;294:11513–24.
31. Farah CA, Sossin WS. The role of C2 domains in PKC signaling. Adv Exp Med Biol. 2012;740:663–83.
32. Alberti S. A phosphoinositide-binding sequence is shared by PH domain target molecules–a model for the binding of PH domains to proteins. Proteins. 1998;31:1–9.
33. Alberti S. HIKE, a candidate protein binding site for PH domains, is a major regulatory region of Gbeta proteins. Proteins. 1999;35:360–3.
34. Manning BD, Toker A. AKT/PKB signaling: navigating the network. Cell. 2017;169:381–405.
35. Freeley M, Kelleher D, Long A. Regulation of protein kinase C function by phosphorylation on conserved and non-conserved sites. Cell Signal. 2011;23:753–62.
36. Tanaka K, Babic I, Nathanson D, Akhavan D, Guo D, Gini B, et al. Oncogenic EGFR signaling activates an mTORC2-NF-κB pathway that promotes chemotherapy resistance. Cancer Discov. 2011. https://doi.org/10.1158/2159-8290.CD-11-0124.
37. Sarbassov DD, Ali SM, Kim DH, Guertin DA, Latek RR, Erdjument-Bromage H, et al. Rictor, a novel binding partner of mTOR, defines a rapamycin-insensitive and raptor-independent pathway that regulates the cytoskeleton. Curr Biol. 2004;14:1296–302.
38. Trerotola M, Ganguly KK, Fazli L, Fedele C, Lu H, Dutta A, et al. Trop-2 is up-regulated in invasive prostate cancer and displaces FAK from focal contacts. Oncotarget. 2015.
39. Trerotola M, Jernigan D, Liu Q, Siddiqui J, Fatatis A, Languino L. Trop-2 promotes prostate cancer metastasis by modulating β1 integrin functions. Cancer Res. 2013;73:3155–67.

40. van Rheenen J, Song X, van Roosmalen W, Cammer M, Chen X, DesMarais V, et al. EGF-induced PIP2 hydrolysis releases and activates cofilin locally in carcinoma cells. J Cell Biol. 2007;179:1247–59.
41. Spratley SJ, Bastea LI, Doppler H, Mizuno K, Storz P. Protein kinase D regulates cofilin activity through p21-activated kinase 4. J Biol Chem. 2011;286:34254–61.
42. Sakuma M, Shirai Y, Yoshino K-I, Kuramasu M, Nakamura T, Yanagita T, et al. Novel PKCα-mediated phosphorylation site(s) on cofilin and their potential role in terminating histamine release. Mol Biol Cell. 2012;23:3707–21.
43. Saczko-Brack D, Warchol E, Rogez B, Kross M, Heissler SM, Sellers JR, et al. Self-organization of actin networks by a monomeric myosin. Proc Natl Acad Sci USA. 2016;113:E8387–95.
44. Choi CK, Vicente-Manzanares M, Zareno J, Whitmore LA, Mogilner A, Horwitz AR. Actin and α-actinin orchestrate the assembly and maturation of nascent adhesions in a myosin II motor-independent manner. Nat Cell Biol. 2008;10:1039–50.
45. Watanabe T, Hosoya H, Yonemura S. Regulation of myosin II dynamics by phosphorylation and dephosphorylation of its light chain in epithelial cells. Mol Biol Cell. 2007;18:605–16.
46. Zanna P, Trerotola M, Vacca G, Bonasera V, Palombo B, Guerra E, et al. Trop-1 are conserved growth stimulatory molecules that mark early stages of tumor progression. Cancer. 2007;110:452–64.
47. Ng T, Shima D, Squire A, Bastiaens PIH, Gschmeissner S, Humphries MJ, et al. PKCα regulates β1 integrin-dependent cell motility through association and control of integrin traffic. EMBO J. 1999;18:3909–23.
48. Zhang XA, Bontrager AL, Hemler ME. Transmembrane-4 superfamily proteins associate with activated protein kinase C (PKC) and link PKC to specific beta(1) integrins. J Biol Chem. 2001;276:25005–13.
49. Jiang X, Teng M, Ji R, Zhang D, Zhang Z, Lv Y, et al. CD9 regulates keratinocyte differentiation and motility by recruiting E-cadherin to the plasma membrane and activating the PI3K/Akt pathway. Biochim Biophys Acta. 2020;1867:118574.
50. Cabantous S, Nguyen HB, Pedelacq J-D, Koraïchi F, Chaudhary A, Ganguly K, et al. A new protein-protein interaction sensor based on tripartite split-GFP association. Sci Rep. 2013;3:2854.
51. Wang H-X, Kolesnikova TV, Denison C, Gygi SP, Hemler ME. The C-terminal tail of tetraspanin protein CD9 contributes to its function and molecular organization. J Cell Sci. 2011;124:2702–10.
52. Sveen A, Ågesen TH, Nesbakken A, Rognum TO, Lothe RA, Skotheim RI. Transcriptome instability in colorectal cancer identified by exon microarray analyses: associations with splicing factor expression levels and patient survival. Genome Med. 2011;3:32.
53. Ågesen TH, Sveen A, Merok MA, Lind GE, Nesbakken A, Skotheim RI, et al. ColoGuideEx: a robust gene classifier specific for stage II colorectal cancer prognosis. Gut. 2012;61:1560.
54. Ambrogi F, Fornili M, Boracchi P, Trerotola M, Relli V, Simeone P, et al. Trop-2 is a determinant of breast cancer survival. PLoS ONE. 2014;9:e96993.
55. Stoyanova T, Goldstein AS, Cai H, Drake JM, Huang J, Witte ON. Regulated proteolysis of Trop2 drives epithelial hyperplasia and stem cell self-renewal via beta-catenin signaling. Genes Dev. 2012;26:2271–85.
56. Mochly-Rosen D, Gordon AS. Anchoring proteins for protein kinase C: a means for isozyme selectivity. FASEB J. 1998;12:35–42.
57. Murayama Y, Shinomura Y, Oritani K, Miyagawa J, Yoshida H, Nishida M, et al. The tetraspanin CD9 modulates epidermal growth factor receptor signaling in cancer cells. J Cell Physiol. 2008;216:135–43.
58. Powner D, Kopp Petra M, Monkley Susan J, Critchley David R, Berditchevski F. Tetraspanin CD9 in cell migration. Biochem Soc Trans. 2011;39:563–7.
59. Hoshino A, Kim HS, Bojmar L, Gyan KE, Cioffi M, Hernandez J, et al. Extracellular vesicle and particle biomarkers define multiple human cancers. Cell. 2020;182:1044–61.e18.
60. Krishn SR, Singh A, Bowler N, Duffy AN, Friedman A, Fedele C, et al. Prostate cancer sheds the αvβ3 integrin in vivo through exosomes. Matrix Biol. 2019;77:41–57.
61. Ciccarelli F, Acciarito A, Alberti S. Large and diverse numbers of human diseases with HIKE mutations. Hum Mol Genet. 2000;9:1001–7.
62. Antal CE, Hudson AM, Kang E, Zanca C, Wirth C, Stephenson NL, et al. Cancer-associated protein kinase C mutations reveal kinase's role as tumor suppressor. Cell. 2015;160:489–502.
63. Sanjana NE, Shalem O, Zhang F. Improved vectors and genome-wide libraries for CRISPR screening. Nat Methods. 2014;11:783–4.
64. Bahmad HF, Cheaito K, Chalhoub RM, Hadadeh O, Monzer A, Ballout F, et al. Sphere-formation assay: three-dimensional in vitro culturing of prostate cancer stem/progenitor sphere-forming cells. Front Oncol. 2018;8:347.
65. Scott RW, Hooper S, Crighton D, Li A, Konig I, Munro J, et al. LIM kinases are required for invasive path generation by tumor and tumor-associated stromal cells. J Cell Biol. 2010;191:169–85.
66. Di Baldassarre A, D'Amico MA, Izzicupo P, Gaggi G, Guarnieri S, Mariggiò MA, et al. Cardiomyocytes derived from human cardiopoieticamniotic fluids. Sci Rep. 2018;8:12028.

## ACKNOWLEDGEMENTS

We thank G. Vacca, F. Dini, E. Eleuterio, and S. Angelucci for help during the course of this work. We also thank C. Berrie for language editing of the paper.

## AUTHOR CONTRIBUTIONS

MT, VR, RT, AS, KH, PS, EG, MC, and and ALA performed the biochemical and functional assays; RLS, RL, NT, and MP collected the human tumor samples, assembled tissue microarrays, and performed IHC analysis; DV. performed the 2D-PAGE and the NanoLC-MS/MS assays; DV, IF, and MS analyzed the data from NanoLC and MS/MS assays; MT and SA planned the study and wrote the paper.

## FUNDING

Italian Ministry of Health (RicOncol RF-EMR-2006-361866), Italian Ministry of Development—FESR 2016–2018. SSI000651, art. 69 Reg. (CE) n. 1083/2006 and Reg. (CE) n. 1828/2006, Region Abruzzo (POR FESR 2007–2013: Activity 1.1.1 line B) C78C14000100005, Oncoxx Biotech, Italy and Marie Curie Transfer of Knowledge Fellowship—EC VI Framework Program (Contract 014541) to SA. Programma Per Giovani Ricercatori "Rita Levi Montalcini", Italian Ministry of University and Research (Grant PGR12I7N1Z) to MT. EG is an inventor in patents WO201687651 and WO201784763, and a partner in Mediterranea Theranostic Srl. MT is an inventor in patent WO201784763. SA is an inventor in patents WO201089782, WO201687651, and WO201784763, and is founder and CEO of Oncoxx Biotech Srl and Mediterranea Theranostic Srl. VR was an employee of Oncoxx Biotech Srl. PS is an inventor in a patent application under consideration (EP3546948).

## COMPETING INTERESTS

The authors declare no competing interests.

## ETHICS APPROVAL

All procedures involving animal care were approved by the Interuniversity Animal Research Ethics Committee (CEISA), Chieti-Pescara and Teramo Universities (Prot. 26/2011/CEISA/PROG/16), and were conducted in compliance with consensus international protocols (D.L. No. 116, G.U. Feb. 18,1992; No. 8, G.U. July, 1994; UKCCCR Guidelines for the Welfare of Animals in Experimental Neoplasia; EEC Council Directive 86/609, Dec. 12,1987; Guide for the Care and Use of Laboratory Animals, US-NRC,1996). Studies on human tumor samples were approved by the Italian Ministry of Health (RicOncol RF-EMR-2006-361866).

## ADDITIONAL INFORMATION

**Supplementary information** The online version contains supplementary material available at https://doi.org/10.1038/s41388-022-02220-1.

**Correspondence** and requests for materials should be addressed to Marco Trerotola or Saverio Alberti.

**Reprints and permission information** is available at http://www.nature.com/reprints

**Publisher's note** Springer Nature remains neutral with regard to jurisdictional claims in published maps and institutional affiliations.